Eur. Phys. J. B (2018) 91: 136
https://doi.org/10.1140/epjb/e2018-90164-y

THE EUROPEAN PHYSICAL JOURNAL B

Regular Article

How sharply does the Anderson model depict a single-electron transistor?*

Krissia Zawadzki and Luiz N. Oliveira[a]

Instituto de Física de São Carlos, University of São Paulo, Cx. Postal 369, 13560-970 São Carlos, SP, Brazil

Received 13 March 2018 / Received in final form 30 April 2018
Published online 2 July 2018

Abstract. The single-impurity Anderson model has been the focus of theoretical studies of molecular junctions and the single-electron transistor, a nanostructured device comprising a quantum dot that bridges two otherwise decoupled metallic leads. The low-temperature transport properties of the model are controlled by the ground-state occupation of the quantum dot, a circumstance that recent density-functional approaches have explored. Here we show that the ground-state dot occupation also parametrizes a linear mapping between the thermal dependence of the zero-bias conductance and a universal function of the temperature scaled by the Kondo temperature. Careful measurements by Grobis and co-workers are very accurately fitted by the universal mapping. Nonetheless, the dot occupation and an asymmetry parameter extracted from the same mapping are relatively distant from the expected values. We conclude that mathematical results derived from the model Hamiltonian reproduce accurately the universal physical properties of the device. In contrast, non-universal features cannot be reproduced quantitatively. To circumvent this limitation, ab initio studies of the device at high energies seem necessary, to accurately define the model Hamiltonian. Our conclusion reinforces findings by Gross and coworkers, who applied time-dependent density-functional theory to show that, to describe the low-energy properties of molecular junctions, one must be able to describe the high-energy regime.

1 Introduction

Molecular junctions and analogous elementary nanostructured devices have motivated a great deal of experimental and theoretical research [1–4]. Archetypical among such systems is the single-electron transistor (SET), a quantum dot or molecule (*dot*, for briefness) bridging two otherwise decoupled 2D electron gases or metallic leads (*leads*) [5–8]. That the single-impurity Anderson Hamiltonian would model the transport properties of the device was realized well before the first SET was manufactured. Two corollaries emerged. First, in view of the universal properties of the Anderson Hamiltonian, quantitative interpretation of experimental data was envisaged. Second, given that the dot occupation controls the ground-state transport properties, the model invited Density-Functional Theory (DFT) treatment. With the invitation, alas, came a challenge.

A formidable barrier faces density-functional theorists interested in molecular junctions or SETs. A crossover separates the high-energy properties from the low-energy properties. The crossover is refractory to perturbative treatment. Only special methods can treat it.

At first, difficulties other than the crossover attracted attention [9]. DFT is centrally concerned with the ground state; research was therefore focused on the low-temperature behavior, the transport properties being computed via Landauer-Büttiker formalism [10]. With a view to developing trustworthy approximations for the exchange-correlation functional, accurate special results such as Density-Matrix Renormalization-Group data [11], the Friedel sum rule [12], the behavior of an isolated impurity in the low-temperature limit [13], and Bethe-Ansatz results for the ground-state occupancy of the Anderson-model impurity [14,15] were invoked.

In this charged environment, the obstacle that lay ahead might have been disregarded, had Hardy and collaborators not issued the heads up. In an inspiring report, they showed that, unlike static DFT, the time-dependent formalism (TD-DFT) can climb the crossover [16], i.e., it can describe the high-energy region, from which the system inherits its low-energy properties. In the wake of this news came a sequence of developments that opened inroads towards the solution of the non-equilibrium problem [13,17–20].

This remarkable progress notwithstanding, some of the work that was done after reference [16] came to light

* Contribution to the Topical Issue "Special issue in honor of Hardy Gross", edited by C.A. Ullrich, F.M.S. Nogueira, A. Rubio, and M.A.L. Marques.

[a] e-mail: luizno@usp.br

indicates that Hardy's message has not come across clearly. Another shot seems in order.

The complexity of the crossover and its relation to high- and to the low-temperature properties can be perceived from another perspective, rooted in physical considerations. The crossover is due to the formation of the Kondo cloud. At high energies, if the gate voltage attracts an odd number of electrons, the dot acquires a magnetic moment. The dot moment is antiferromagnetically coupled to the moments of the nearby lead electrons. As the temperature T is lowered past a characteristic temperature T_K (the Kondo temperature, typically of the order of 1 K), a cloud arises in the leads that couples with the dot spin to form a singlet. Below T_K, the entanglement between the dot and lead electrons allows ballistic conduction across the device.

The cloud is large. The correlation length grows as the temperature is reduced, i.e., as the Hamiltonian crosses over from the high- to the low-temperature regimes, and may exceed $1\,\mu$. Such long lengths introduce non-local effects that simple approximations to the static exchange-correlation functional are unlikely to capture. Discussion of the DFT approach from a strategical perspective seems therefore warranted. Along that line of reasoning, the crossover merits special attention.

To express the transition mathematically, it is convenient to examine the temperature-dependent transport properties of the model Hamiltonian. Here, we show that the thermal dependence of the zero-bias electrical conductance maps linearly onto a universal function. To show that the mapping is robust, we consider asymmetries often found in experiments: typically, the device lacks inversion symmetry because the dot is more strongly coupled to one of the leads than to the other, and it lacks particle-hole symmetry because external potentials are applied to the leads. We show that, even under such asymmetric conditions, the thermal dependence of the conductance maps linearly onto the universal function. Equally important for the purposes of our discussion, the mapping is parametrized by the ground-state expectation value for the dot occupation.

How reliable is this universal relation? The mapping has been thoroughly checked against Numerical Renormalization-Group data [21]. The accurate experimental data reported by Grobis et al. [22] pose a more trying test. Reference [22] systematically applied a sequence of gate voltages at various temperatures to span the Kondo regime. We fit the thermal dependence at each gate voltage with the universal expression and extrapolate the experimental data to temperatures $T \gg T_K$ and the $T \ll T_K$. The extrapolations determine the conductance at temperatures well outside the experimentally accessible thermal range. They also determine the Kondo temperature and ground-state dot occupations as functions of the gate potential. The comparison shows that the universal properties of the model Hamiltonian reproduce the experimental data quantitatively. By contrast, the nonuniversal properties agree but qualitatively with parameters derived from the experimental results.

We conclude that accurate diagonalization of a simplified Hamiltonian is sufficient to describe the crossover to the low-temperature regime, while ab initio treatment is necessary to describe other aspects of the experiment. To draw attention to the practical implications of this conclusion, we recall the renormalization-group argument showing that the high-energy spectrum is approximately reproduced by a single-particle Hamiltonian devoid of characteristic energies [23]. The similar spectra open an opportunity for DFT descriptions of the device at high energies, which can be combined with a nonperturbative treatment of the crossover to reach the low-temperature regime.

The paper is structured as follows. Section 2 defines the model Hamiltonian and cursorily derives the general expression for the zero-bias conductance. Section 3 discusses the characteristics energies of the model and the special regimes they define and then discusses the mapping of the conductance to a universal function. Section 4 shows that the mapping fits experimental data quantitatively and compares the resulting dot occupancies with expected values. A summary section caps the text.

2 Conductance

Our analysis slightly extends the work of Yoshida et al. [21], who showed that the thermal dependence of the SET conductance in the Kondo regime maps linearly to a universal function of the temperature scaled by the Kondo temperature. The linear coefficient is a trigonometric function of the ground-state phase-shift induced by the screening of the dot moment. Here, we will allow for an external potential applied to the leads and take advantage of Friedel's sum rule to relate the phase shift to the $T \ll T_K$ and the $T \gg T_K$ occupations of the dot orbital.

The schematic drawing in Figure 1 defines the model. (For a micrograph of the modeled device, see Fig. 1a in Ref. [22].) The quantum dot, at the center of the figure, is coupled to the left (L) and the right (R) leads with couplings V_L and V_R, respectively. The dot-level energy, and hence the dot occupancy are controlled by the gate potential V_G.

The Anderson Hamiltonian modeling the device in Figure 1 reads

$$H_A = H_d + \sum_{k,\alpha=L,R} \epsilon_k c^\dagger_{k\alpha} c_{k\alpha} + \sum_{k,q,\alpha=L,R} \frac{W_{k,q}}{N} c^\dagger_{k\alpha} c_{q\alpha} + \sum_{\alpha=L,R} \frac{V_\alpha}{\sqrt{N}} (c^\dagger_d c_{k\alpha} + \text{H. c.}) \quad (1)$$

with implicit spin sums throughout. As usual, the dot Hamiltonian H_d comprises a Coulomb repulsion U and a dot energy V_G, defined by the gate potential. The half-filled conduction bands in the first term on the right-hand side represent the left- ($\alpha = L$) and the right-hand ($\alpha = R$) leads. Since we are interested in low-energy properties, it is appropriate to consider a linear dispersion relation $\epsilon_k = v_F k$, where v_F is the Fermi velocity, and the momenta k (energies ϵ_k) are measured from the Fermi

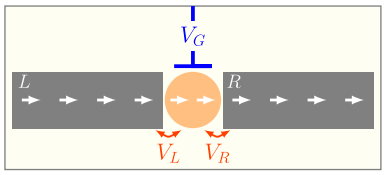

Fig. 1. Single-electron transistor. The quantum dot is asymmetrically coupled to the left (L) and the right (R) leads, with couplings V_L and V_R, respectively. The gate potential V_G controls the dot energy. The arrows indicate the direction of conduction.

momentum (level). The ϵ_k form a band of width 2D. The normalized sum $(1/\sqrt{N})\sum_{k\alpha} c_{k\alpha}$ defines the Wannier state in lead α to which the dot level c_d is coupled.

The third term on the right-hand side of equation (1) represents the external potentials that experimentalists apply to the leads to control the electronic density. To maintain equilibrium, equal potentials must be applied. The form in equation (1) represents a potential with arbitrary position dependence. Simplification is nonetheless possible with essentially no accuracy loss, as we now explain.

Renormalization-group theory shows that substitution of a constant W for the momentum-dependent coefficients $W_{q,k}$ in the third term on the right-hand side of equation (1) adds only irrelevant terms to the Hamiltonian [23,24]. In more physical language, the substitution introduces deviations of $O(k_BT/D)$, where k_B is Boltzmann's constant. As the temperature is lowered, such deviations become small. For temperatures such that $k_BT \ll D$, which typically cover the entire Kondo crossover, they can be safely disregarded.

Substitution of W for $W_{k,q}$ reduces equation (1) to the form

$$H_A = H_d + \sum_{k,\alpha=L,R} \epsilon_k c^\dagger_{k\alpha} c_{k\alpha} + \frac{W}{N} \sum_{k,q,\alpha=L,R} c^\dagger_{k\alpha} c_{q\alpha} + \sum_{\alpha=L,R} \frac{V_\alpha}{\sqrt{N}} (c^\dagger_d c_{k\alpha} + \text{H. c.}), \quad (2)$$

mathematically equivalent to having the external potential applied to the Wannier orbitals coupled to the dot.

2.1 Decoupling of the model Hamiltonian

It is straightforward to construct linear combinations of the operators $c_{k\alpha}$ ($\alpha = L, R$) that are decoupled from the quantum dot [25]. To this end we define the orthonormal Fermi operators

$$a_k = \frac{V_L c_{kL} + V_R c_{kR}}{V}, \quad (3)$$

$$b_k = \frac{V_R c_{kL} - V_L c_{kR}}{V}, \quad (4)$$

where

$$V \equiv \sqrt{V_L^2 + V_R^2}. \quad (5)$$

Projected on the basis of a_k's and b_k's, the Hamiltonian (1) reduces to the form

$$H_A = H + \bar{H}, \quad (6)$$

where

$$\bar{H} = \sum_k \epsilon_k b^\dagger_k b_k + \frac{W}{N} \sum_{k,q} b^\dagger_k b_q, \quad (7)$$

and

$$H = H_d + \sum_k \epsilon_k a^\dagger_k a_k + W f^\dagger_0 f_0 + V(c^\dagger_d f_0 + \text{H. c.}), \quad (8)$$

with the shorthand

$$f_0 = \frac{1}{\sqrt{N}} \sum_k a_k. \quad (9)$$

The right-hand side of equation (8) is the standard expression for the single-impurity, single-band Anderson Hamiltonian [26]. The second band, defined by equation (7), is decoupled from the quantum dot and can be disregarded, for nearly all applications. Exceptions are the transport properties, to which the b_k's contribute. To compute the zero-bias electrical conductance, for example, one must apply an infinitesimal bias

$$H_\mu = \Delta\mu \sum_k \left(c^\dagger_{kR} c_{kR} - c^\dagger_{kL} c_{kL} \right), \quad (10)$$

which shifts the chemical potential at the R (L) lead by $\Delta\mu$ ($-\Delta\mu$).

Projection of equation (10) upon the basis defined by equation (3) shows that H_μ couples the a_k's to the b_k's. Likewise, the current operator $\hat{I} = d\hat{q}_R/dt$, where $\hat{q}_R$ is the electrical charge in lead R, couples the a_k's to the b_k's. Standard linear response theory links the conductance G to the commutator between the bias Hamiltonian H_μ and the current $\hat{I}$.

When the quantum dot is symmetrically coupled to the two leads, the model Hamiltonian remains invariant under left-right inversion, and parity is conserved. In that case, equations (3) and (4) define operators that are even and odd under inversion, respectively. The algebra that determines $[H_\mu, \hat{I}]$ for $V_R = V_L$ and derives an expression for the conductance has been spelled out in Appendix C of reference [21]. The extension of that analysis to unequal couplings on the basis of equations (3)–(10)

is straightforward and yields the result

$$G(T) = \kappa\pi\mathcal{G}_2\Gamma_W \int \left(-\frac{\partial f}{\partial\epsilon}\right)\rho_d(\epsilon)\,d\epsilon. \tag{11}$$

Here $\rho_d(\epsilon)$ is the c_d-level spectral density, $f(\epsilon)$ is the Fermi function,

$$\mathcal{G}_2 \equiv \frac{2e^2}{hc} \tag{12}$$

is the quantum conductance with two spin channels,

$$\Gamma_W \equiv \frac{\pi\rho V^2}{1+\pi^2\rho^2W^2}, \tag{13}$$

where $\rho \equiv 1/D$ is the conduction-band density of states, and

$$\kappa \equiv \frac{4V_L^2V_R^2}{V^4}. \tag{14}$$

The asymmetry index κ is a dimensionless factor that modulates the conductance. The modulus is unitary for symmetric couplings, $V_L = V_R$, and shrinks as the coupling asymmetry grows. To simplify the following theoretical analysis, we define the *reduced conductance*

$$\bar{G} \equiv \frac{G}{\kappa}, \tag{15}$$

so that equation (11) reads

$$\bar{G}(T) = \pi\mathcal{G}_2\Gamma_W \int \left(-\frac{\partial f}{\partial\epsilon}\right)\rho_d(\epsilon)\,d\epsilon. \tag{16}$$

3 Characteristic energies and fixed points

The spectral density ρ_d is a function of energy and temperature. Since the Hamiltonian (7) is decoupled from the dot, we only have to diagonalize H to compute ρ_d and determine the conductance from equation (16). The computation is simple in special regimes, defined by the characteristic energies of the Hamiltonian.

In the absence of the potential W, the coupling to the leads broadens the dot level to the width

$$\Gamma = \pi\rho V^2. \tag{17}$$

The potential W reduces the broadening, as indicated by equation (13).

If the width Γ were zero, the dot occupation would be conserved. The dynamics of the device would then be controlled by the eigenvalues E_d^ℓ ($\ell = 0, 1, 2$) of H_d. The d^0 eigenstate would have energy $E_d^0 = 0$, the $d_\uparrow^1$ and $d_\downarrow^1$ eigenstates (where the subscript indicates the S_z eigenvalue) would have energy $E_d^1 = V_G$, and the d^2 eigenstate would have energy $E_d^2 = 2V_G + U$.

We are centrally interested in the gate-voltage range making E_d^1 smaller than E_d^0 and E_d^2, i.e., in the range $0 > V_G > -U$. In this interval, the dot acquires a magnetic moment μ_B. The interval is limited by the two *charge-degeneracy points*, associated with the voltages $V_G^{0\to1} = 0$, which makes $E_d^0 = E_d^1$, and $V_G^{1\to2} = -U$, which makes $E_d^1 = E_d^2$. At the middle of the interval is the *symmetric point*, attained with gate voltage $V_G^1 = -U/2$.

With no coupling, conduction would be impossible. With small coupling $\Gamma_W \ll |V_G|$, $\Gamma_W \ll U$, charge transport is barred by an energy barrier $\Delta E_c = \min\{|V_G|, U + V_G\}$, except within a gate-voltage range of width Γ_W of either charge-degeneracy point. The barrier ΔE_c is known as the *Coulomb blockade*.

At moderately high temperatures, such that thermal energy k_BT lies in the interval $\Delta E_c \gg k_BT \gg T_K$, the width Γ can be disregarded, the dot occupation is approximately conserved, and the Coulomb blockade controls the physics of conduction—the Coulomb blockade regime. Assuming that the width D of the conduction bands exceeds U, we can see that the thermal energy is incommensurate with the other energy scales of the problem. Physically, the model Hamiltonian is then approximately equivalent to the *local-moment fixed-point* Hamiltonian H_{LM}^* obtained by letting $D, U \to \infty$, $V_G \to -\infty$, and $\Gamma \to 0$ in equation (8).

The local-moment fixed-point Hamiltonian is equivalent to a dot with unitary occupation and magnetic moment μ_B decoupled from conduction band of non-interacting electrons. The fixed-point Hamiltonian reads

$$H_{LM}^* = \sum_k \epsilon_k a_k^\dagger a_k + W f_0^\dagger f_0, \tag{18}$$

where the superscript reminds us that the fixed-point Hamiltonian is devoid of characteristic energies.

H_{LM}^* is an idealized Hamiltonian whose many-body spectrum is approximately equal to the energy spectrum of the Hamiltonian H in the range $\Delta E_c \gg \epsilon \gg \Gamma_W$. The dot level makes no contribution to the right-hand side. Still, the dot level has a spin-1/2 degree of freedom, which we will denote $\vec{S}$.

The conduction band is phase shifted by the potential W, i.e., each single-particle eigenstate acquires a phase shift δ_W, given by the expression

$$\tan\delta_W = -\pi\rho W. \tag{19}$$

Depending on W, the phase shift can take any value in the interval $-\pi/2 < \delta \le \pi/2$. The LM fixed-point Hamiltonian can be visualized as a point with phase shift δ along a line running from $-\pi/2$ to $\pi/2$.

3.1 Kondo Hamiltonian

The fixed point is an idealization. In practice, neither U, nor $|V_G|$ are infinite. Even at (moderately) high

temperatures, the Hamiltonian H is not exactly the fixed-point Hamiltonian. The high-energy many-body spectrum of H^*_{LM} is only an approximation to the spectrum of H, because the finite Coulomb barriers allow virtual excitations to the d^0 and d^2 dot states.

The virtual excitations induce an antiferromagnetic coupling between the dot magnetic moment and the magnetic moments of the conduction electrons [27]. A more precise representation of the high-energy spectrum of H comes therefore from the equation

$$H_K = \sum_k \epsilon_k a_k^\dagger a_k + \tilde{W} f_0^\dagger f_0 + J\vec{S}\cdot\sum_{\mu,\nu}\vec{\sigma}_{\mu\nu} f_{0\mu}^\dagger f_{0\nu}, \quad (20)$$

where the components of $\vec{\sigma}$ are the Pauli matrices, and the coefficientes of the second and third terms on the right-hand side are given by the Schrieffer-Wolff expressions [27]

$$\rho\tilde{W} = \rho W + \frac{\Gamma/\pi}{V_G} + \frac{\Gamma/\pi}{V_G + U}, \quad (21)$$

and

$$\rho J = \frac{\Gamma/\pi}{|V_G|} + \frac{\Gamma/\pi}{V_G + U}. \quad (22)$$

Equation (20) defines the Kondo Hamiltonian. For thermal energies that are small on the scale of the Coulomb blockade, the spectra of H and H_K are approximately congruent. The right-hand sides of equations (21) and (22) become very large in absolute value near the charge degeneracy points $V_G = 0$ and $V_G = -U$.

Near the symmetric point, by contrast, as long as $\Gamma \ll U$ there is a range of gate voltages such that $\Gamma \ll |V_G|$ and $\Gamma \ll U + V_G$. That gate-voltage range makes $\rho J \ll 1$ and places the device in the *Kondo regime*.

The symmetric point lies at the middle of the gate-voltage interval associated with the Kondo regime. At the symmetric point, the second and third terms on the right-hand side of equation (21) cancel each other, and the phase shift equals δ_W. Elsewhere within the Kondo regime, the phase shift is given by the equality

$$\tan\delta_0 = -\pi\left(\rho W + \frac{\Gamma}{V_G} + \frac{\Gamma}{V_G + U}\right). \quad (23)$$

Physically, the phase shift is associated with the screening charge in the vicinity of the f_0 orbital, due to the potential W and to the coupling to the quantum dot.

3.2 Frozen-level fixed point

If the device is cooled in the Kondo regime, at sufficiently low temperatures the antiferromagnetic interaction between the conduction elctrons and the dot spin will induce the Kondo cloud. At temperatures well below the Kondo temperature, the dot spin will lock into a singlet with the conduction-electron spins, which will freeze the dot-spin degree of freedom.

As a result, at low thermal energies, with $T \ll T_K$, the spectrum of H approaches that of the Hamiltonian obtained from equation (20) when we let $J \to \infty$. The f_0 orbital then forms a singlet with the dot spin variable, and the Hamiltonian becomes equivalent to the quadratic form

$$H^*_{FL} = \sum_k \bar{\epsilon}_k \bar{a}_k^\dagger \bar{a}_k + \tilde{W}\sum_{k,q}\bar{a}_k^\dagger \bar{a}_q, \quad (24)$$

where the set of the conduction states $\bar{a}_k$ and the localized orbital f_0 form an orthonormal basis that is complete relative to the original conduction states a_k. The subscript on the left-hand side reminds us that the dot level is frozen, and the superscript, that H^*_{FL} is devoid of characteristic energies.

To be orthogonal to f_0 the new conduction states $\bar{a}_k$ must deplete the region of the leads next to the quantum dot. They must therefore be phase-shifted by $\pi/2$ relative to the a_k. It follows that the conduction energies $\bar{\epsilon}_k$ are shifted relative to the ϵ_k. Since the conduction band, of width $2D$, accommodates N levels, the ϵ_k are split by $\Delta\epsilon_k = D/(2N)$. Since $\rho = 1/D$, the shifted energy levels are given by the expression

$$\rho\bar{\epsilon}_k = \rho\epsilon_k - \frac{1}{4N}, \quad (25)$$

and the FL fixed-point phase shift, by the expression

$$\delta = \frac{\pi}{2} + \delta_0, \quad (26)$$

where δ_0 is the LM fixed-point phase shift.

3.3 Fixed-point conductances

To determine the conductance from equation (16), we must compute the spectral density $\rho_d(\epsilon)$. An exact expression relates $\rho_d(\epsilon)$ to the spectral densities of the linear combinations $\sum_k a_k$ and $\sum_k \epsilon_k a_k$ of the conduction operators c_k [21,28]. As the model Hamiltonian approaches a fixed point, the latter two spectral densities can be computed from the eigenvalues and eigenstates of the fixed-point Hamiltonian. The diagonalization of the fixed-point, single-particle Hamiltonians H^*_{LM} and H^*_{FL} is straightforward. It is therefore a simple matter to obtain the fixed-point spectral densities [21]

$$\rho_d^* = \frac{1}{\pi\Gamma_W}\sin^2(\delta_* - \delta_W), \quad (T \gg T_K \text{ or } T \ll T_K), \quad (27)$$

where δ_* denotes the fixed-point phase shift.

For $W = 0$, the phase shift δ_W vanishes, and we recover Langreth's expression for the low-energy spectral density [29]. Equation (27) is valid at low ($T \ll T_K$) and at high ($T \gg T_K$) energies. However, since the LM and the FL fixed points have distinct phase-shifts, the spectral densities at high and at low energies are different.

Substitution of the fixed-point results in equation (16) now yields the following expression for the fixed-point conductances:

$$\bar{G}^* = \mathcal{G}_2 \sin^2(\delta_* - \delta_W). \tag{28}$$

3.4 Thermal dependence of the conductance

With $W = 0$, the zero-bias conductance at the symmetric point is a universal function of the temperature scaled by the Kondo temperature [30,31]:

$$\bar{G}(T) = \mathcal{G}_2 G_S(T/T_K). \tag{29}$$

Figure 2 displays the universal function G_S as a function of the ratio T/T_K. The condition $G_S(T = T_K) = \mathcal{G}_2/2$ defines the Kondo temperature. At high (low) temperatures, the Hamiltonian is close to the LM (FL) fixed point, and the conductance, close to zero ($\mathcal{G}_2$). Physically, for $T \gg T_K$ the coupling J between the dot and the conduction-electron spins is so weak that the dot moment is virtually decoupled from the leads. At the symmetric point $V_G = -U/2$ the Coulomb blockade imposes the energy barrier $\Delta E_c = U/2$, much larger than the thermal energy. Conduction across the device is virtually impossible.

As the temperature is lowered, the Kondo cloud starts forming. As T drops past T_K the electrons within the cloud bind into a singlet with the dot electron. The binding is so tight that it allows ballistic transport.

3.4.1 Particle-hole symmetry

The symmetric point is special. With $W = 0$ and $V_G = -U/2$, the Hamiltonian (8) remains invariant under the particle-hole transformation

$$\begin{aligned} c_d &\to -c_d^\dagger; \\ c_k &\to c_q^\dagger. \end{aligned} \tag{30}$$

Here, the momenta k and q are symmetric: given k, one chooses q such that $\epsilon_q = -\epsilon_k$.

The particle-hole transformation inverts the sign of the phase shift δ. Consequently, the fixed-point phase shifts of the symmetric Hamiltonian can only be $\delta = 0$ or $\delta = \pi/2$. At the high-temperature (LM) fixed point the phase shift vanishes; at the low-temperature (FL) fixed point $\delta = \pi/2$. It follows from equation (28) that, at the symmetric point, $\bar{G}^*_{LM} = 0$ and $\bar{G}^*_{FL} = \pi/2$, as indicated by the high- and low-temperature limits in Figure 2.

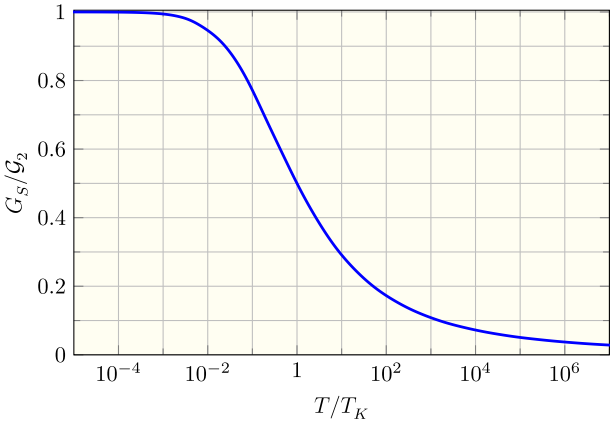

Fig. 2. Universal function relating the SET conductance at the symmetric point $V_G = -U/2$ to the temperature scaled by the Kondo temperature.

3.4.2 Linear mapping

Deviation from the symmetric condition $V_G = -U/2$ or application of a potential W breaks particle-hole symmetry. Depending on the model parameters, the fixed-points phase shifts can now take any values in the $[-\pi/2, \pi/2]$ interval. The LM (FL) conductance will no longer be zero ($\mathcal{G}_2$). Clearly, $\bar{G}(T/T_K)$ cannot follow the plot in Figure 2, nor can it be proportional to $G_S(T/T_K)$.

Instead, the conductance maps linearly onto the universal function [21,32]:

$$\bar{G}\Big(\frac{T}{T_K}\Big) = \alpha G_S\Big(\frac{T}{T_K}\Big) + \beta. \tag{31}$$

To determine the linear coefficients α and β, we go back to equation (28). At the FL fixed point, the phase shift is δ, and the universal conductance reaches $\mathcal{G}_2$ as $T \to 0$. Equation (31) then reads

$$\mathcal{G}_2 \sin^2(\delta - \delta_W) = \alpha \mathcal{G}_2 + \beta. \tag{32}$$

At the LM fixed point, the phase shift is $\delta_0 = \delta - \pi/2$, and the universal conductance vanishes in the large T limit. Equation (31) therefore reads

$$\mathcal{G}_2 \cos^2(\delta - \delta_W) = \beta. \tag{33}$$

Substitution on the right-hand side of equation (32) determines α and brings equation (31) to the explicit form

$$\bar{G}\Big(\frac{T}{T_K}\Big) - \frac{\mathcal{G}_2}{2} = \left(\frac{\mathcal{G}_2}{2} - G_S\Big(\frac{T}{T_K}\Big)\right) \cos 2(\delta - \delta_W). \tag{34}$$

At the symmetric point, with $W = 0$ the FL phase shift is $\delta = \pi/2$, and equation (34) reduces to equation (29). Elsewhere in the parametrical space of the model, the trigonometric function on the right-hand side is larger

than −1. The high-temperature (low-temperature) conductance is then positive (smaller than $\mathcal{G}_2$). At the Kondo temperature, the conductance is always $\mathcal{G}_2/2$, but the difference between $\bar{G}^*_{FL}$ and $\bar{G}^*_{LM}$ may be significantly smaller than $\mathcal{G}_2$.

3.4.3 Phase shifts and occupation

The Friedel sum rule relates the fixed-point phase shifts to the ground-state dot occupation n_d. At the FL fixed point, n_d is proportional to the phase shift induced by the coupling to the leads. If there were no coupling, the phase shift would be δ_W. The induced shift is therefore $\delta_* - \delta_W$. According to the Friedel sum rule [29], then,

$$n_d = \frac{2(\delta_* - \delta_W)}{\pi}. \tag{35}$$

Equation (34) can now be rewritten in the form

$$\bar{G}\Big(\frac{T}{T_K}\Big) - \frac{\mathcal{G}_2}{2} = \left(\frac{\mathcal{G}_2}{2} - G_S\Big(\frac{T}{T_K}\Big)\right)\cos(\pi n_d), \tag{36}$$

which shows that the thermal dependence of the conductance is parametrized by the ground-state expectation value for the dot occupancy.

Since the model Hamiltonian comprises potentials applied to the leads and dot, from the Hohenberg-Kohn Theorem [33] we expect its eigenstates and eigenvalues, and hence its physical properties to depend on the ground-state electronic densities at the leads and orbital occupation at the dot. Equation (36) goes one step beyond and states that, even with potentials applied to the leads, the conductance at given temperature scaled by the Kondo temperature is a functional of the ground-state dot occupation only.

4 Comparison with experiment

In the Kondo regime, equation (36) is exact. It is instructive to compare it with the experimental data reported in reference [22]. Equation (15), which relates the experimental conductance $G(T)$ to the reduced conductance $\bar{G}(T)$, yields the following expressions for the high- and low-temperature limits of the experimental conductance:

$$G_{LM} = \kappa\mathcal{G}_2\cos^2\Big(\frac{\pi n_d}{2}\Big), \tag{37}$$

and

$$G_{FL} = \kappa\mathcal{G}_2\sin^2\Big(\frac{\pi n_d}{2}\Big). \tag{38}$$

At intermediate temperatures, the experimental conductance maps linearly onto the universal function. From equation (36) it follows that

$$G\Big(\frac{T}{T_K}\Big) - \kappa\frac{\mathcal{G}_2}{2} = \left(\frac{\mathcal{G}_2}{2} - G_S\Big(\frac{T}{T_K}\Big)\right)\kappa\cos(\pi n_d). \tag{39}$$

4.1 Experimental data

Grobis et al. [22] have measured the conductance of a single-electron transistor as a function of temperature, gate voltage, and bias voltage. We focus on their zero-bias results. To scan a Kondo plateau, the authors have accurately measured G on a $V_G \times T$ grid comprising 34 uniformly spaced gate-voltages, ranging from −212.5 mV to −196 mV, and 17 temperatures, ranging from 13 mK to 205 mK. Figure 1c in reference [22] overviews the resulting data. At fixed gate-voltage, the conductance rises as the sample is cooled, from approximately $0.5\mathcal{G}_2$ at $T = 205$ mK to approximately $0.85\,\mathcal{G}_2$ at $T = 13$ mK. The rise is steeper at the middle of the plateau, around $V_G = -205$ mV.

Qualitatively, we can see that equation (39) agrees with these features of the data. In fact, the agreement is quantitative, as illustrated by Figure 3. Each panel plots the measured conductance G as a function of the universal conductance G_S for the depicted gate voltage. As long as the temperature is scaled by the Kondo temperature, we expect the relation between the two conductances to be linear.

Since T_K is unknown, we proceed by trial and error. The experimental temperatures are scaled by a trial Kondo temperature, and linear regression determines the optimum coefficient $\kappa\cos(\pi n_d)$ and intercept $\kappa\mathcal{G}_2/2$ fitting $G(T/T_K)$ to $G_S(T/T_K)$. If the linear correlation coefficient is sufficiently close to unity, we have found the Kondo temperature. Otherwise, we turn to Newton's method for a better estimate of T_K, and repeat the procedure. Convergence yields the Kondo temperature and the coefficients of the linear fit.

This procedure was applied to the thermal dependence of the conductance at each gate voltage in the experimental grid. In each case, the agreement was comparable to the fits in Figure 3.

As the plots in Figure 3 show, the straight lines can be extrapolated to the $G_S \to \mathcal{G}_2$ ($G_S \to 0$) limit to yield the FL (LM) fixed-point conductance G_{FL} (G_{LM}). Linear regression therefore determines the high- and the low-temperature limits of the conductance, which are inaccessible in the laboratory.

Figure 4 shows all $34 \times 17 \equiv 578$ experimental conductances, measured from $G(T_K) = \mathcal{G}_2/2$, scaled by the difference $G(0) - G(T_K)$ between the extrapolated low-temperature conductance and the Kondo-temperature conductance, as a function of the temperature scaled by T_K. To identify the gate-voltage at which each conductance was measured, the inset shows the 34 Kondo temperatures as a function of V_G. The near congruence between the symbols and the solid line representing the

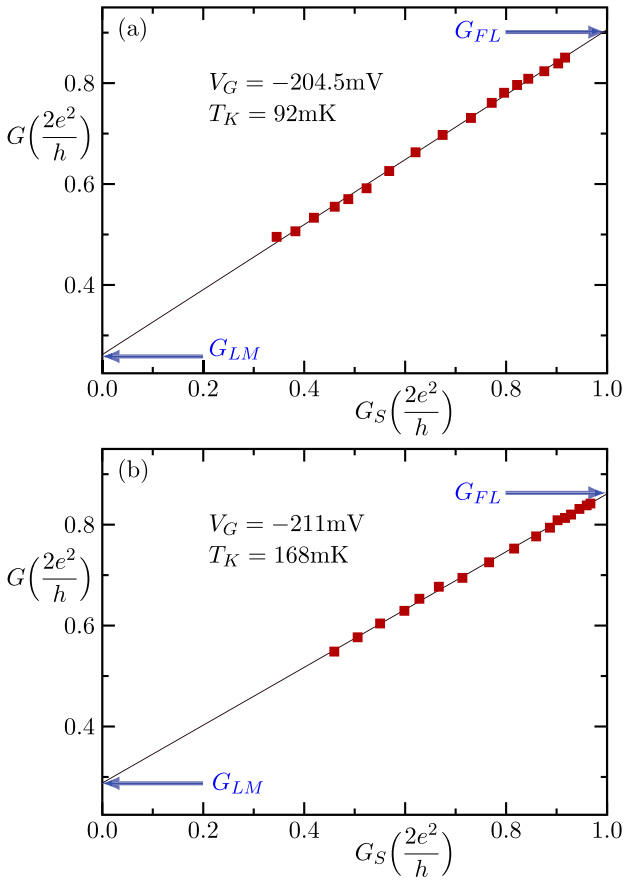

Fig. 3. Conductance $G(T/T_K)$ as a function of the universal function $G_S(T/T_K)$. The filled squares in (a) and (b) show the conductances measured in reference [22] for the indicated gate voltages at 17 temperatures ranging from $T = 12.5$ mK (point closest to the upper right corner) to $T = 203$ mK (closest to the bottom left corner). In each plot, the indicated Kondo temperature optimizes the linear regression of $G(T/T_K)$ vs. $G_{\rm SET}(T/T_K)$, depicted by a solid line. The horizontal arrows labeled G_{FL} and G_{LM} point to the low- and high-temperature limits of the conductance, respectively.

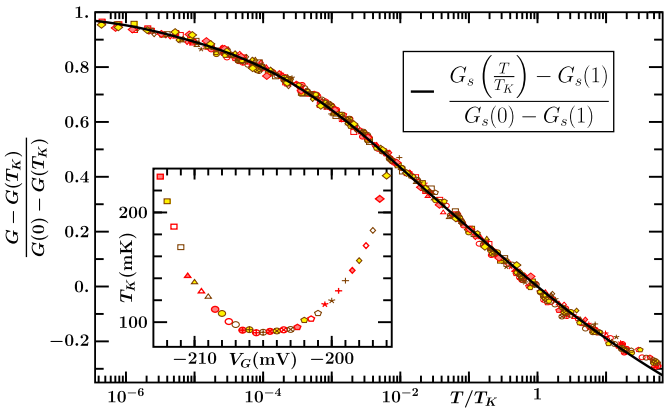

Fig. 4. Scaled zero-bias conductance $G(T)$ (symbols) and universal function $G_S(T/T_K)$ (solid line), as functions of T/T_K. Each symbol represents the former for one of the 34 gate voltages V_G in reference [22]. In the inset, the same symbol shows the corresponding T_K.

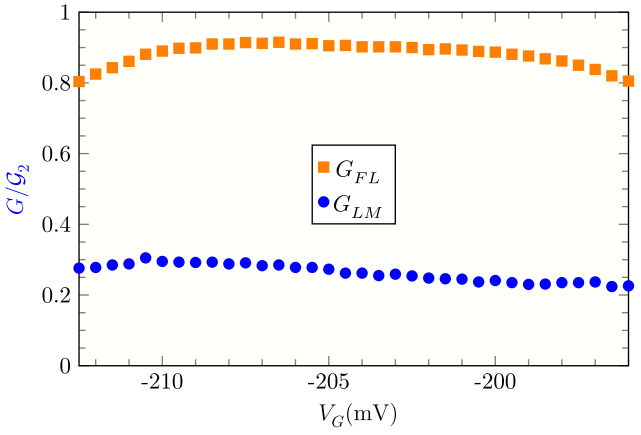

Fig. 5. Fixed-point conductances G_{LM} and G_{FL} as functions of the gate voltage V_G. At each gate voltage, the LM and FL fixed-point conductances result from extrapolating the $G(T/T_K)$ *vs.* $G_S(T/T_K)$ plots to $G_S = 0$ and $G_S = 1$, respectively, as illustrated by each panel in Figure 4.

universal function scaled in the same fashion offers a measure of the overall harmony between the measurements and the expected universal behavior in the Kondo regime.

Figure 5 shows the resulting estimates of G_{FL} and G_{LM} as functions of the gate voltage. At each gate-voltage, the limit conductances determine the ground-state expectation value n_d of the dot occupancy and the asymmetry index κ. To obtain n_d from equations (37) and (38), we compute the ratio

$$\frac{G_{FL}}{G_{LM}} = \tan^2\left(\frac{\pi n_d}{2}\right). \tag{40}$$

To obtain the asymmetry index we compute the sum

$$\frac{G_{FL}}{\mathcal{G}_2} + \frac{G_{LM}}{\mathcal{G}_2} = \kappa. \tag{41}$$

The resulting ground-state dot occupancy n_d and asymmetry index κ are depicted in Figure 6, as functions of the gate voltage V_G. Both plots have unexpected features. In the Kondo regime, the ground-state dot occupancy should be close to unity. Instead, the blue dots in the figure span an interval ranging from $n_d = 0.66$ to $n_d = 0.70$. The asymmetry index, expected to be a constant $\kappa \leq 1$, varies between $\kappa = 1.03$ and $\kappa = 1.20$.

We conclude that the Hamiltonian (1) cannot describe the device in reference [22] quantitatively. Given the simplicity of the model, which neglects electron-electron interactions within the leads, considers identical, structureless, half-filled conduction bands, adopts a single level to represent the quantum dot, and gives no attention to the spatial dependence of the potentials applied to the leads or to the momentum dependence of the couplings between the dot and the leads, the conclusion seems hardly surprising.

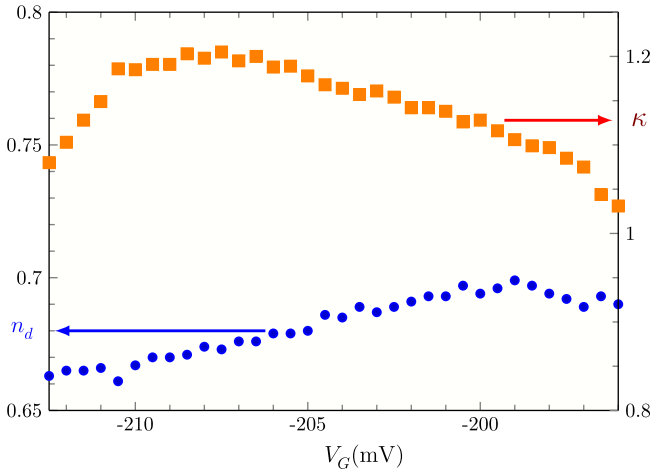

Fig. 6. Coupling asymmetry index κ and ground-state dot-level occupation n_d as functions of the gate voltage V_G. At each gate voltage, equation (41) determines κ, while equation (40) determines n_d.

More puzzling is the contrast between the deviations of Figure 6 from the expected behavior and the much superior agreements in Figures 3 and 4. The puzzle, however, can be easily unraveled. Recall that equation (30), besides exact in the Kondo regime, is universal. Other properties of the Anderson model, such as the mathematical connection between the physical features of the device and the LM Hamiltonian, are nonuniversal. The minimalist, inaccurate description of the physical features is responsible for the deviations in Figure 6, while universality protects the fits in Figures 3 and 4 from such inaccuracies.

This underscores the call for ab initio treatment of the device. Consider, for definiteness, the experimental data by Grobis et al. [22]. While static DFT approaches may be unable to deal with the crossover from the LM to FL fixed points, even local approximations to the exchange-correlation functional should be sufficient to describe the LM fixed point and determine the LM conductance. Comparison with the solid blue circles in Figure 5 would then test our understanding of the physics underlying the experimental data.

To examine the same argument from a different perspective, consider a local-density description of the LM fixed point associated with the model Hamiltonian (8). H^*_{LM} is given by equation (18). Since the model conduction electrons are noninteracting, the exchange-correlation potential vanishes inside the leads. The Kohn-Sham eigenstates are the single-particle eigenstates of H^*_{LM}. DFT therefore yields the phase shift $\delta = \delta_W$. From equations (15) and (28), the conductance is predicted to vanish at high temperatures, in the Kondo regime. At the symmetric point, this agrees with the plot in Figure 2. The prediction nonetheless disagrees, conspicuously, with the blue solid circles in Figure 5.

DFT cannot be blamed for the disagreement. True, the local-density approximation neglects the antiferromagnetic interaction with the dot spin and hence misses the contribution from the last term on the right-hand side of equation (20) and the contribution to $\tilde{W}$ from the last two terms on the right-hand side of equation (21). In the Kondo regime, however, those terms are small. They cannot account for the substantial conductances represented by the blue solid circles in Figure 5.

The discrepancy is due to the shortcomings of the model, not to the limitations of the local-density approximation for the exchange-correlation functional. To strengthen the argument, we substitute $\tilde{W}$ (given by Eq. (21)) for W on the right-hand side of equation (18). A more accurate approximation results, which takes the spin-independent phase shift induced by dot moment into account. Notwithstanding the improvement, the resulting conductance is still zero at the symmetric point, which corresponds to $V_G \approx -205\,\mathrm{mV}$ in the experimental setup [22].

With or without the correction to DFT introduced by the last two terms on the right-hand side of equation (21) the model fails to account for the relatively large LM conductances resultant from the extrapolations of the experimental data. A mored realistic description of the experimental device, i.e., a description based on ab initio treatment is necessary to describe the LM fixed point.

5 Summary

The single-electron transistor poses a concrete challenge to DFT. Recent progress, backed by improved local approximations for the exchange-correlation functional especially designed to yield the correct density derivative, have yielded accurate descriptions of the ground-state conductance for the Anderson Hamiltonian. Unfortunately, this approach has only been proven successful in the region where it must give satisfactory results by construction [18,34].

To propose an alternative static approach, we have combined concepts drawn from renormalization-group theory with the notion that the thermal dependence of the SET conductance is parametrized by the ground-state expectation value for the quantum-dot occupation. Chiefly important in this context is the progressive formation of the screening cloud in the Kondo regime as the Hamiltonian crosses over from a high- to a low-energy fixed points. At high temperatures, the dot possesses a magnetic moment. At low temperatures, the dot spin forms a singlet with the conduction electrons.

Renormalization-group theory associates the high-energy spectrum of the Anderson Hamiltonian with the many-body spectrum of the local-moment fixed-point Hamiltonian H^*_{LM}, and the low-energy spectrum with that of the frozen-level fixed-point H^*_{FL}. At intermediate energies, which correspond to the temperature range over which the dot magnetic moment is screened, the model Hamiltonian crosses over from the vicinity of H^*_{LM} to the vicinity of H^*_{FL}.

The physical properties describing the SET crossover are universal. In particular, as discussed in Section 3.4, the electrical conductance maps linearly onto a universal function of the temperature scaled by the Kondo temperature T_K. The mapping is controlled by the dot occupancy n_d.

The linear mapping fits the experimental data by Grobis et al. [22] with very small deviations. Nonetheless, the resulting dot occupancies n_d are substantially lower than unity, and the asymmetry index of the device κ is gate-voltage dependent and exceeds unity.

The thermal dependence of the conductance for the Anderson model in the Kondo regime reproduces the experimental data very well, while non-universal aspects of the same model offer a blurred picture of the SET constructed by Grobis et al. [22]. Ab initio treatment of the device is therefore necessary before quantitative description of the experimental data becomes possible. Given that universality simplifies the description of the crossover from the high- to the low-temperature fixed points, ab initio description of the high-energy fixed point will suffice.

From a practical viewpoint, this is convenient, for in contrast with the crossover the high-energy region yields to perturbative treatment [23]. Moreover, the high-energy fixed point having no characteristic energy scales, its properties are temperature independent. The ground-state energy of H^*_{LM} can therefore be computed by standard DFT methods.

By contrast, the crossover to the FL fixed point calls for special, non-perturbative mathematical procedures. In this context, only the the Bethe-Ansatz [35] and the numerical renormalization-group [21,30,31] approaches have yielded exact or essentially exact results. The remaining challenge is to adapt one of those two methods, so that the DFT treatment of the high-energy spectrum can serve as input for the non-perturbative description of the crossover. Current work is addressing that problem [36].

Three decades ago, Hardy Gross showed the ropes of DFT to one of us (LNO). In exchange, he requested a talk on the Kondo problem, which was never materialized. So here it is, Hardy, at long last. Too little, and too late, but drawn from the heart, in memory of the grand time. Close your eyes, for a second, and you may see Walter and the two of us gathered around his table, lit by the setting sun and a hundred flickering rays coming from the blue waters of the Pacific. Thanks for those moments, and for all that I have learned from you. Live long, Hardy, and leads us farther.

We are grateful to Mike Grobis for sending us the experimental data and thank Harold Baranger and Vivaldo Campo for very helpful discussions at an early stage of this work. The FAPESP (grant 2012/02702-0) and CNPq (grants 312658/2013-3 and 401414/2014-0) have supported the research.

Author contribution statement

K.Z. did the numerical work, including fits to the experimental results, and collaborated with L.N.O in the analytical derivations and write-up.

References

1. H. Bouchiat, Y. Gefen, S. Guéron, G. Montambaux, J. Dalibard (Eds.), *Nanophysics: coherence and transport* (Elsevier, Amsterdam, 2005)
2. Y.V. Nazarov, Y.M. Blanter, *Quantum transport: introduction to nanoscience* (Cambridge University Press, Cambridge, 2009)
3. G. Stefanucci, R. van Leeuwen, *Nonequilibrium many-body theory of quantum systems: a modern introduction* (Cambridge University Press, Cambridge, 2013)
4. M. Thoss, F. Evers, J. Chem. Phys. **148**, 030901 (2018)
5. L.I. Glazman, M.E. Raikh, JETP Lett. **47**, 452 (1987)
6. D. Goldhaber-Gordon, H. Shtrikman, D. Mahalu, D. Abusch-Magder, U. Meirav, M.A. Kastner, Nature **391**, 156 (1998)
7. D. Goldhaber-Gordon, J. Gores, M.A. Kastner, H. Shtrikman, D. Mahalu, U. Meirav, Phys. Rev. Lett. **81**, 5225 (1998)
8. T.K. Ng, P.A. Lee, Phys. Rev. Lett. **61**, 1768 (1988)
9. H. Mera, Y.M. Niquet, Phys. Rev. Lett. **105**, 216408 (2010)
10. M. Büttiker, Phys. Rev. Lett. **57**, 1761 (1986)
11. P. Schmitteckert, F. Evers, Phys. Rev. Lett. **100**, 086401 (2008)
12. P. Tröster, P. Schmitteckert, F. Evers, Phys. Rev. B **85**, 115409 (2012)
13. G. Stefanucci, S. Kurth, Phys. Rev. Lett. **107**, 216401 (2011)
14. J.P. Bergfield, Z.-F. Liu, K. Burke, C.A. Stafford, Phys. Rev. Lett. **108**, 066801 (2012)
15. Z.-F. Liu, J.P. Bergfield, K. Burke, C.A. Stafford, Phys. Rev. B **85**, 155117 (2012)
16. S. Kurth, G. Stefanucci, E. Khosravi, C. Verdozzi, E.K.U. Gross, Phys. Rev. Lett. **104**, 236801 (2010)
17. S. Kurth, G. Stefanucci, Phys. Rev. B **94**, 241103 (2016)
18. S. Kurth, G. Stefanucci, J. Phys.: Condens. Matter **29**, 413002 (2017)
19. D. Jacob, S. Kurth, Nano Lett. **18**, 2086 (2018)
20. S. Kurth, D. Jacobs, arXiv:1803.06307[cond-mat.mes-hall] (2018)
21. M. Yoshida, A.C. Seridonio, L.N. Oliveira, Phys. Rev. B **80**, 235317 (2009)
22. M. Grobis, I.G. Rau, R.M. Potok, H. Shtrikman, D. Goldhaber-Gordon, Phys. Rev. Lett. **100**, 246601 (2008)
23. K.G. Wilson, Rev. Mod. Phys. **47**, 773 (1975)
24. H.R. Krishna-murthy, J.W. Wilkins, K.G. Wilson, Phys. Rev. B **21**, 1003 (1980)
25. M. Pustilnik, L. Glazman, J. Phys.: Condens. Matter **16**, R513 (2004)
26. P.W. Anderson, Phys. Rev. **124**, 41 (1961)
27. J.R. Schrieffer, P.A. Wolff, Phys. Rev. **149**, 491 (1966)
28. J.W.M. Pinto, L.N. Oliveira, Comput. Phys. Commun. **185**, 1299 (2014)
29. D.C. Langreth, Phys. Rev. **150**, 516 (1966)
30. T. Costi, A. Hewson, V. Zlatic, J. Phys.: Condens. Matter **6**, 2519 (1994)
31. R. Bulla, T.A. Costi, T. Pruschke, Rev. Mod. Phys. **80**, 395 (2008)
32. A.C. Seridonio, M. Yoshida, L.N. Oliveira, Europhys. Lett. **86**, 67006 (2009)
33. P. Hohenberg, W. Kohn, Phys. Rev. **136**, B864 (1964)
34. S. Kurth, G. Stefanucci, Phys. Rev. Lett. **111**, 030601 (2013)
35. A.M. Tsvelick, P.B. Wiegmann, Adv. Phys. **32**, 453 (1983)
36. K. Zawadzki, L.N. Oliveira, Combined density-functional theory/numerical renormalization group approach to the computation of transport properties. Unpublished